(Received 12 June 2025, Accepted 20 August 2025, Scheduled 3 September 2025)

A Class of Asymmetric Microstrip Hybrid Couplers with Enhanced Bandwidth and Isolation Using Multi Section Phase Shifters for Modern Microwave Systems

Shubham Tirmanwar* and Debapratim Ghosh

School of Electrical and Computer Sciences, IIT Bhubaneswar, Odisha 752050, India

ABSTRACT: This paper presents a class of wideband hybrid couplers with enhanced isolation, based on an N-section phase shift filter network integrated into an unequal-split, multi-section branch-line hybrid architecture. The key innovation lies in the incorporation of the N-section phase shift network, which significantly enhances the fractional bandwidth with each increase in section and isolation performance compared to conventional designs. A detailed design methodology applicable for any N is developed and validated through the fabrication and testing of two microstrip prototypes for $N = 3$ and $N = 4$ at a center frequency of 1 GHz. Both simulated and measured results confirm consistent tight coupling, insertion loss better than 6 dB, and isolation exceeding 15 dB across all prototypes. Furthermore, $N = 3$ and $N = 4$ hybrids show peak isolation of 87.4 dB, 96.8 dB in simulation and 66.5 dB, 72.7 dB in measurement, respectively, at the center frequency of 1 GHz. Notably, the designs demonstrate a progressive improvement in the fractional bandwidth, achieving 73.68% and 91.89% for $N = 3$ and $N = 4$, respectively. This scalable and frequency-flexible design approach makes the proposed class of hybrid couplers highly suitable for modern microwave systems such as vector network analyzer (VNA) test set, applications in radar, communication receivers, and phased array antennas.

1. INTRODUCTION

A hybrid coupler is an important element in the field of microwave engineering, playing a crucial role in various applications such as power splitting, combining, and power amplifier stages. Furthermore, it is used in Vector Network Analyzers (VNAs) for isolating incident and reflected waves at the load, as well as in radar transceivers [1]. Considering the applications of couplers which need to provide the required signal division, a good hybrid coupler must provide tight coupling and high isolation over a broad bandwidth. Most of the couplers reported in literature often compromise either one or two of coupling level, isolation level, and bandwidth, in order to improve the other metrics, which is outlined as follows.

Among the reported works aimed at improving isolation and/or directivity, various approaches have been explored. An optimization-based design achieves 20 dB coupling, 40 dB directivity, and a 53% fractional bandwidth (FBW) with center frequency 2 GHz, demonstrating a well-balanced trade-off between directivity and bandwidth [2]. Another approach utilizing a phase control unit improves isolation to better than 10 dB, but in doing so, the design sacrifices bandwidth, achieving a significantly narrower operating frequency range from 3.2 to 3.8 GHz and 17.1% FBW [3]. A GaAs MMIC coupler that incorporates an adaptive bridged-T equalizer demonstrates isolation above 40 dB across a wide frequency range from 2 GHz to 20 GHz. However, this design exhibits loose 20 dB coupling, which may limit its applicability in scenarios requiring tighter coupling levels [4]. For millimeter-wave applications, PRGW (Periodic Ridge Gap Waveguide) technology achieves over 15 dB isolation and minimum measurement loss of 0.7 dB with FBW of 26.5% at 30 GHz center frequency, offering a reasonable balance between isolation and bandwidth [5]. In another approach, a semi-flexible coaxial coupler delivers an impressive 35 dB directivity over a wide frequency range of 5 MHz to 150 MHz. However, this design suffers from loose coupling at 45 dB but manages to minimize insertion loss less than 0.65 dB, making it less suitable for applications demanding stronger power division [6].

Several reported designs aim to provide arbitrary phase shifts while maintaining more than 10 dB isolation, though the trade-offs in other performance metrics vary across different implementations [7–10]. A hybrid coupler with phase reconfigurable transmission line is reported in [11]. It shows isolation, return loss above 10 dB and coupling, insertion loss better than 6 dB over frequency range 2.2 to 2.6 GHz. The reported literature collectively indicates that achieving high isolation and/or directivity often necessitates loosening the coupling strength or sacrificing bandwidth, which presents a fundamental design challenge.

On the other hand, several techniques have been developed to maintain tight coupling while improving performance. For instance, multi-hole differential waveguide couplers achieve a coupling of 3 dB, with isolation exceeding 20 dB, over 12.85 to 20.7 GHz frequency range and FBWs ranging from 46.8% to 67% [12]. Another technique utilizing folded coupled lines

* Corresponding author: Shubham Tirmanwar (tsl11@iitbbs.ac.in).

effectively enhances performance within similar coupling and isolation parameters with center frequency 2 GHz [13]. Additionally, designs that eliminate impedance discontinuities have been shown to improve bandwidth while preserving a tight coupling configuration with center frequency 1.5 GHz [14]. Further advancements in ridge-gap waveguide technology offer tunable coupling values ranging from 3 dB to 33 dB, while maintaining a minimum isolation of 20 dB [15]. In [16], a 4 dB directional coupler is implemented by incorporating inclined longitudinal slots between the substrate layers, achieving an isolation better than 14 dB and a fractional bandwidth of 7.1%. In dual-band coupled-line designs, a 3 dB coupling level is achieved alongside 15 dB isolation and an FBW of 37.8%, making these designs suitable for multi-band applications [17]. Another approach involves patch-based filtering hybrid couplers, which sustain 3 dB coupling with over 20 dB isolation and maximum 1.31 dB insertion loss. However, these designs exhibit a narrow FBW 20.9% at 4.21 GHz and 9.5% at 6.39 GHz, which limits their broadband usability [18]. Additional 3 dB hybrid coupler designs have been explored, particularly those using cascaded sections to reduce overall circuit size while preserving key performance parameters [19, 20]. A high-impedance transmission line coupler achieves 15 dB isolation and an FBW of 23.67%, offering a balance between performance and compactness [21]. Another design, using a rectangular-section coupler, maintains 3 dB coupling with 20 dB isolation and 3 dB insertion loss, but only over a narrow frequency band with center frequency 2.27 GHz [22]. Meanwhile, a microstrip design incorporating low-pass filters (LPFs) achieves 3 dB coupling but with 20 dB isolation, while benefiting from a compact footprint suitable for integration into modern RF systems [23]. A hybrid lumped-element coupler, designed for lower-frequency applications, delivers 10 dB isolation and 3.5 dB coupling, operating effectively over a frequency range of 400 MHz to 600 MHz [24].

To summarize, previously reported designs often trade off bandwidth, coupling, isolation, and/or directivity. Several classical papers [25, 26] propose tightly coupled multi-branch hybrids; however, they are often not suitable for planar microstrip realization. To address this, the proposed paper presents a new class of asymmetric hybrid couplers using N-section phase shifters, achieving tight 6 dB coupling, high isolation above 15 dB, and improved bandwidth. Section 2 describes the detailed, stepwise design of the proposed class of asymmetric hybrid couplers, demonstrating tight coupling with high isolation over improved bandwidth. Section 3 presents the simulated and measured results of the hybrid. Section 4 concludes the paper.

2. PROPOSED DESIGN METHODOLOGY

Figure 1 illustrates the block diagram of the proposed class of asymmetric hybrid couplers. The hybrid uses an N-section phase shift filter circuit, where N is the number of sections. Port 1 functions as the input port of the hybrid coupler; Ports 2 and 4 serve as the coupled and through ports respectively; and Port 3 is the isolated port of the hybrid coupler. The complete coupler comprises four sections: a power divider, a phase shift filter circuit, an unequal-split branch line hybrid coupler,

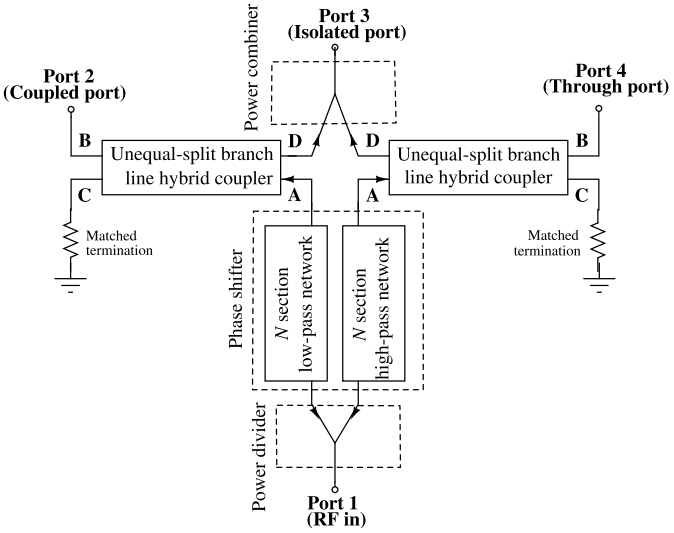

FIGURE 1. Block diagram of the proposed class of N-section tightly coupled asymmetric hybrid couplers.

and a power combiner circuit. The approach is to generate two out-of-phase waves from a single input at Port 1, ensuring maximum signal level at the coupled and through ports. Furthermore, when these waves combine, perfect phase cancellation will occur, resulting in minimal signal reaching Port 3 and thereby maximizing the isolation. To achieve this, the first stage uses a power divider to split the signal into two equal-amplitude signals. Next, a phase shift circuit is included in the second stage to introduce the necessary phase difference (in this design, chosen as $180°$) over the desired frequency range, which will be used later for phase cancellation. Furthermore, N-section phase-shift filter circuits are realized to increase the bandwidth over which the $180°$ phase difference is obtained. In the third stage, unequal split branch line hybrid couplers are used to achieve maximum signal at Port 2 (coupled port) and Port 4 (through port) of the proposed hybrid coupler to ensure 6 dB coupling. This is because unlike symmetric hybrids, which rely on uniform fixed coupling across all arms, an asymmetric design allows for required tight coupling levels to achieve desired power-splitting ratios. Finally, a power combiner is used in the fourth stage to feed the out-of-phase signals ultimately emanating from the branch line hybrid coupler, thereby ensuring perfect phase cancellation and achieving high isolation at Port 3 with respect to Port 1. A detailed design analysis applicable for any N is developed and validated through the fabrication and testing of two microstrip prototypes for $N = 3$ and $N = 4$ at a center frequency of 1 GHz. In the following subsections, the detailed design and working of the individual stages is explained.

2.1. Wilkinson Divider and Combiner Stages

As shown in Figure 1 to realize the power divider, the initial stage employs a conventional Wilkinson divider [27] to generate two signals with identical phase. Round-shaped arms are utilized to minimize line bend losses. In the final stage, the same Wilkinson divider circuit is used as a combiner to merge the two out-of-phase signals. Both Wilkinson divider and com-

biner are designed at the center frequency of 1 GHz. The actual layouts of the Wilkinson divider and combiner are shown in Figure 8 at the end of Section 2.

2.2. N-Section Phase Shift Filter Circuit

The second stage contains the phase shift filter circuit, which comprises two filters in two arms: a low pass filter (LPF) and a high pass filter (HPF) as shown in Figure 2. The intended phase difference between the outputs of the phase-shifter circuit, i.e., the filters' outputs, is 180°. Both the LPF and HPF are realized in the form of an N-section network, using a series of a series of π-section LC networks. This structure is developed by extending the basic lumped π circuit in [28]. Due to the multiple sections, it increases the prospect of improved bandwidth with each additional section. The values of the inductors and capacitors are calculated using the $ABCD$ parameters of each LPF/HPF network and equating them to those of a transmission line providing the requisite phase shift. The analysis starts with the individual $ABCD$ matrices for each of the shunt and series components in both the LPF and HPF arms, followed by combining the series sections to form a single $ABCD$ matrix. The resulting $ABCD$ parameters are as follows:

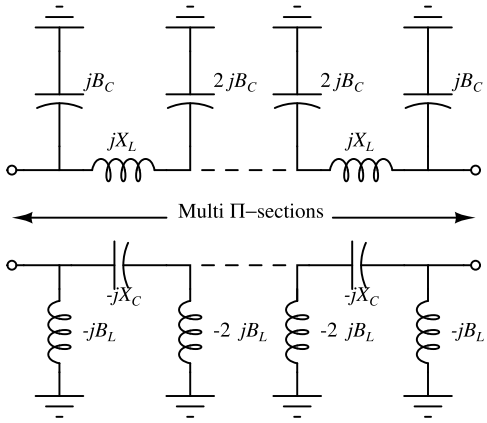

FIGURE 2. Proposed N-section phase shift filter circuit employing low and high pass filter branches.

For the low pass filter circuit:
Single section $(N = 1)$:

$$\begin{bmatrix} A & B \\ C & D \end{bmatrix}_1 = \begin{bmatrix} 1 & 0 \\ jB_C & 1 \end{bmatrix} \begin{bmatrix} 1 & jX_L \\ 0 & 1 \end{bmatrix} \begin{bmatrix} 1 & 0 \\ jB_C & 1 \end{bmatrix} \quad (1)$$

Two sections $(N = 2)$:

$$\begin{bmatrix} A & B \\ C & D \end{bmatrix}_2 = \begin{bmatrix} 1 & 0 \\ jB_C & 1 \end{bmatrix} \begin{bmatrix} 1 & jX_L \\ 0 & 1 \end{bmatrix} \begin{bmatrix} 1 & 0 \\ 2jB_C & 1 \end{bmatrix} \begin{bmatrix} 1 & jX_L \\ 0 & 1 \end{bmatrix} \begin{bmatrix} 1 & 0 \\ jB_C & 1 \end{bmatrix} \quad (2)$$

Three sections $(N = 3)$:

$$\begin{bmatrix} A & B \\ C & D \end{bmatrix}_3 = \begin{bmatrix} 1 & 0 \\ jB_C & 1 \end{bmatrix} \begin{bmatrix} 1 & jX_L \\ 0 & 1 \end{bmatrix} \begin{bmatrix} 1 & 0 \\ 2jB_C & 1 \end{bmatrix} \begin{bmatrix} 1 & jX_L \\ 0 & 1 \end{bmatrix} \begin{bmatrix} 1 & 0 \\ jB_C & 1 \end{bmatrix} \quad (3)$$

Four sections $(N = 4)$:

$$\begin{bmatrix} A & B \\ C & D \end{bmatrix}_4 = \begin{bmatrix} 1 & 0 \\ jB_C & 1 \end{bmatrix} \begin{bmatrix} 1 & jX_L \\ 0 & 1 \end{bmatrix} \begin{bmatrix} 1 & 0 \\ 2jB_C & 1 \end{bmatrix} \begin{bmatrix} 1 & jX_L \\ 0 & 1 \end{bmatrix} \begin{bmatrix} 1 & 0 \\ 2jB_C & 1 \end{bmatrix} \begin{bmatrix} 1 & jX_L \\ 0 & 1 \end{bmatrix} \begin{bmatrix} 1 & 0 \\ jB_C & 1 \end{bmatrix} \quad (4)$$

After solving the above matrices, the expressions for A, B, C, and D parameters are realized as follows:
Single section $(N = 1)$:

$$A = D = 1 - X_L B_C \quad (5)$$
$$B = jX_L \quad (6)$$
$$C = jB_C(2 - X_L B_C) \quad (7)$$

Two sections $(N = 2)$:

$$A = D = 1 - 4X_L B_C + 2{X_L}^2 {B_C}^2 \quad (8)$$
$$B = 2jX_L(1 - X_L B_C) \quad (9)$$
$$C = 2jB_C(1 - X_L B_C)(1 - 2X_L B_C) \quad (10)$$

Three sections $(N = 3)$:

$$A = D = 1 - 9X_L B_C + 12{X_L}^2 {B_C}^2 - 4{X_L}^3 {B_C}^3 \quad (11)$$
$$B = jX_L\left(3 - 9X_L B_C + 4{X_L}^2 {B_C}^2\right) \quad (12)$$
$$C = jB_C\left(6 - 19X_L B_C + 16{X_L}^2 {B_C}^2 - 4{X_L}^3 {B_C}^3\right) \quad (13)$$

Four sections $(N = 4)$:

$$A = D = 1 - 16X_C B_L + 40{X_C}^2 {B_L}^2 - 32{X_C}^3 {B_L}^3 + 8{X_C}^4 {B_L}^4 \quad (14)$$
$$B = -4jX_C\left(1 - 5X_C B_L + 6{X_C}^2 {B_L}^2 - 2{X_C}^3 {B_L}^3\right) \quad (15)$$
$$C = -4jB_L\left(2 - 11X_C B_L + 17{X_C}^2 {B_L}^2 - 10{X_C}^3 {B_L}^3 + 2{X_C}^4 {B_L}^4\right) \quad (16)$$

For each value of N, the corresponding $ABCD$ matrix is equated to that of a transmission line having parameters (Z, θ), with Z being the line impedance and θ being the electrical length of the line, corresponding to the desired LPF/HPF phase shift angle.

$$\begin{bmatrix} A & B \\ C & D \end{bmatrix}_N = \begin{bmatrix} \cos\theta & jZ\sin\theta \\ jY\sin\theta & \cos\theta \end{bmatrix}, \quad (17)$$

where $Y = 1/Z$, as per the phase requirement for the LPF, and the value of $\theta = 90°$ is substituted in (17). To get the required phase for the LPF, the $ABCD$ parameter in (17) must be equal to the $ABCD$ parameter equations mentioned from (5) to (16), as per the selected value of N.

For example, the $ABCD$ equations of the LPF having $N = 1$ from (5) to (7) is equated to (17) with $\theta = 90°$, and the resulting equations in terms of $X_L B_C$ (where X_L is the reactance of the series inductor L, and B_C is the susceptance of the shunt capacitor C) are as follows:

$$1 - X_L B_C = 0 \quad (18)$$

$$jX_L = jZ \tag{19}$$

$$jB_C(2 - X_L B_C) = jY \tag{20}$$

Now substituting the term $X_L B_C = a$ and $Z = 50\,\Omega$ and solving Equation (18) for a, the following solution is obtained:

$$a = X_L B_C = 1 \tag{21}$$

Furthermore, the $ABCD$ equations of the LPF having $N = 2$, from (8) to (10), are equated to (17) with $\theta = 90°$, and the resulting equations in terms of $X_L B_C$ are as follows:

$$1 - 4X_L B_C + 2{X_L}^2{B_C}^2 = 0 \tag{22}$$

$$2jX_L(1 - X_L B_C) = j50 \tag{23}$$

$$2jB_C(1 - X_L B_C)(1 - 2X_L B_C) = j0.02 \tag{24}$$

Now substituting the term $X_L B_C = a$ and $Z = 50\,\Omega$ and solving the quadratic Equation (22) for a, the following two solutions are obtained:

$$a = X_L B_C = 0.29, 1.7 \tag{25}$$

For higher values of N, the higher-order polynomials provide more number of such solutions for a. Since this is a numerical approach, the approximation mentioned in [29] shows that the value of a closer to 0 yields a solution that fits (17) better. Accordingly, $a = X_L B_C = 1$ is chosen for $N = 1$ and $a = X_L B_C = 0.29$ for $N = 2$. For $N = 1$, it is a first order equation, so from Equation (19), $L = 8.05\,\text{nH}$ is obtained, when which is further substituted in (21), $C = 3.14\,\text{pF}$ is obtained. For $N = 2$, putting the value of $a = X_L B_C = 0.29$ in (23) and solving for X_L, $L = 5.55\,\text{nH}$ is obtained, when which is further substituted in (25), $C = 1.32\,\text{pF}$ is obtained. Table 1 shows the obtained and selected solutions for a, which are identical for both the LPF and HPF due to the symmetric nature of the polynomials for both cases. In a similar manner, the values of L and C are calculated for four cases of the N-section low-pass filter (LPF) and N-section high-pass filter (HPF) (with $\theta = -90°$) as shown in Tables 2 and 3, respectively. Using this approach, all the values of inductors and capacitors are determined at 1 GHz. This method proves effective for N-section phase shift filter circuits. Figure 3 shows the simulated phase difference between the LPF and HPF outputs close to 180° for $N = 1...4$. It is observed that with increase in N, the bandwidth over which the phase difference is close to 180° also increases, verifying the proposed approach in this paper for improving the bandwidth.

TABLE 1. Solution of $a = X_L B_C$ or $X_C B_L$ for $N = 1...4$, applicable for both LPF and HPF branches.

	$N=1$	$N=2$	$N=3$	$N=4$
Solutions for a	1	0.29	0.13	0.076
		1.7	1	0.61
			1.86	1.38
				1.92
Selected value of a	1	0.29	0.13	0.076

X_C is the reactance of the series capacitor and B_L is the susceptance of the shunt inductor in the HPF.

TABLE 2. Computed values of L and C for low pass filter circuit of the N-section phase shifter.

	$N=1$	$N=2$	$N=3$	$N=4$
Inductor (L)	8.05 nH	5.55 nH	4.26 nH	3.04 nH
Capacitor (C)	3.14 pF	1.32 pF	0.8 pF	0.636 pF

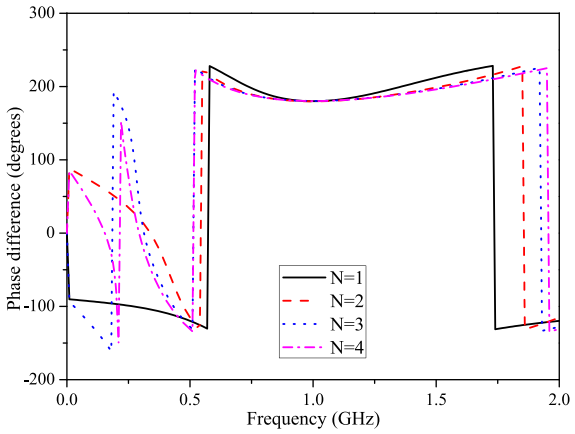

FIGURE 3. Simulated phase difference between LPF and HPF outputs of the phase shifter for number of sections $N = 1...4$.

TABLE 3. Computed values of L and C for high pass filter circuit of the N-section phase shifter.

	$N=1$	$N=2$	$N=3$	$N=4$
Inductor (L)	8.05 nH	19.15 nH	30.4 nH	40.5 nH
Capacitor (C)	3.14 pF	4.52 pF	6.2 pF	8.2 pF

The analysis so far assumes ideal L and C components. However, practical iterations show that even high-Q surface-mount radio frequency (RF) inductors exhibit significant tolerance, parasitics, and drift. Therefore, inductors are implemented as meandered lines for values below 10 nH and circular planar spirals for values above 10 nH [30]. High-SRF (self resonant frequency), high-Q discrete capacitors from Kyocera and Kemet are used, with simulations indicating that the circuit can tolerate up to 5% variation in capacitor values without notable degradation in S-parameters.

2.3. Unequal Split Four Branch Line Hybrid Coupler

Branch line couplers offer significant advantages over coupled line couplers in applications that require broadband performance, high isolation, high power handling capacity [25], and flexible control over power division. Traditional designs of branch line couplers can be found in [25, 26]. It has been observed that increasing the number of sections improves bandwidth, but this also results in extremely high or low values of branch impedance. At a certain point, achieving such impedance becomes impractical in microstrip designs, as the physical dimensions required for such lines are difficult to realize. So a four section branch line hybrid coupler is implemented to obtain the maximum possible bandwidth over which flat coupling for the overall N-section hybrid coupler is achieved.

Compared with traditional four branch line hybrids, the proposed hybrid improves its bandwidth with increase in the section of phase shifter circuit. To avoid confusion with the overall N-section hybrid coupler, the ports of the four branch hybrid coupler are numbered as A, B, C, and D. The general structure of a four branch line hybrid coupler is as follows — main line impedance of Z_s, and branch line impedance of Z_a, Z_b, Z_b, and Z_a in that order.

Using the generalized approach outlined in [31], the characteristic equation of this four branch line hybrid coupler is derived using the following steps:

1. In the even-odd mode analysis of the four-branch line hybrid, the structure is symmetrically divided along the horizontal axis. Even mode assumes equal-magnitude, in-phase waves, creating a virtual open circuit along the symmetry line, while odd mode assumes equal-magnitude, out-of-phase waves, resulting in a virtual short circuit. The analysis is completed by determining the $ABCD$ parameters for individual series and shunt stubs in each mode and multiplying them to obtain the overall $ABCD$ parameters.
2. To convert the $ABCD$ parameters into S-parameters, the $ABCD$ matrix is first used to determine the even- and odd-mode reflection (Γ_e, Γ_o) and transmission coefficients (T_e, T_o), as outlined in [32].
3. The obtained S-parameter expressions are then be equated to the expected values ($S_{AA} = S_{DA} = 0$) to obtain perfect isolation. To satisfy $S_{AA} = S_{DA} = 0$, the condition $\Gamma_e = \Gamma_o = 0$ is required for the even and odd modes. Solving for $\Gamma_e = 0$ using the $ABCD$ parameters the coupler design equation is obtained as:

$$\left(\frac{{Z_s}^3}{{Z_b}^2 Z_0} - \frac{Z_s}{Z_0} + \frac{Z_0}{Z_s}\right) Z_a^2 - \left(\frac{2Z_s Z_0}{Z_b}\right) Z_a + \left(\frac{{Z_s}^3 Z_0}{{Z_b}^2} - Z_s Z_0\right) = 0 \quad (26)$$

Figure 4 shows the variation of Z_a with respect to Z_s for different fixed values of Z_b that satisfy (26). For higher values of Z_s, higher values of Z_a are obtained, which become too large to realize in microstrip form. Equation (26) is valid for only the condition of perfect port impedance match and isolation. It does not govern the power levels going to the coupled Port B and through Port C of the hybrid coupler. Since the proposed four-branch hybrid coupler is intended to function as the phase shifter shown in Fig. 1, an equal-split 3 dB branch line hybrid would result in a net coupling level at Port 2 to be 6 dB or worse (3 dB from the Wilkinson divider and phase shifter, and 3 dB from the hybrid). The case for the through port would be similar, i.e., Port 4. Thus, to make the coupling and through port power levels for the overall proposed hybrid coupler higher, the four branch line hybrid is designed with unequal power splits such that more power goes to Port B (-1.5 dB), as compared to Port C (-5.33 dB). The additional advantage is that Port D (isolated port) of the branch-line hybrid is connected to Port 3 through Wilkinson power combiner to enable monitoring reflected signals from Port 2, which is essential for reflectometry-based applications. This configuration allows Port 3 to function as a reflected power detection port. When the device under test (DUT) connected at Port 2 is mismatched, a portion of the signal reflects back, and due to the phase characteristics of the hybrid structure, this reflected signal constructively adds at Port 3. Conversely, for a perfectly matched DUT, the reflected waves from the coupler branches cancel out at Port 3 due to their out-of-phase nature, resulting in minimal signal. It makes Port 3 critical for evaluating DUT matching conditions and is particularly useful in applications such as six-port reflectometers or vector network analyzer (VNA) test sets. Furthermore, the higher insertion loss of the four branch hybrid will indirectly sent less power to Port 3 of the overall hybrid coupler, resulting in improved isolation.

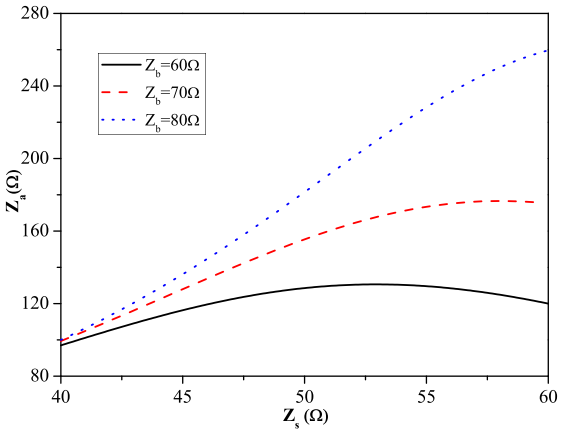

FIGURE 4. Variation of Z_a with Z_s for different values of Z_b that satisfy Equation (26).

Figure 6 shows the analytical values of $|S_{BA}|$ and Z_a when Z_b is varied for fixed value of Z_s from which the impedance solutions are obtained. The desired result is obtained for $Z_s = 45\,\Omega$, with $Z_a = 127.56\,\Omega$, and $Z_b = 70.01\,\Omega$. Higher Z_s results in higher branch impedances, while lower Z_s results in higher Z_b and lower S_{BA}. Thus, fixing the value of Z_s and solving for Z_a and Z_b, the solutions obtained and corresponding dimensions are presented in Table 4. Fig. 7 shows the S_{BA} and through S_{CA} parameters (corresponding to the coupling and insertion loss respectively) simulated using Cadence AWR Microwave Office, for FR4 substrate ($\epsilon_r = 4.4$, $h = 1.6$ mm, $\tan\delta = 0.02$). It is observed that at the center frequency of

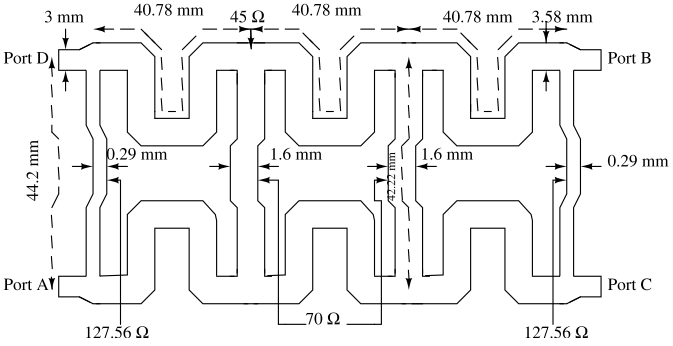

FIGURE 5. Complete layout of the unequal split 4-branch line hybrid coupler with meandered branches.

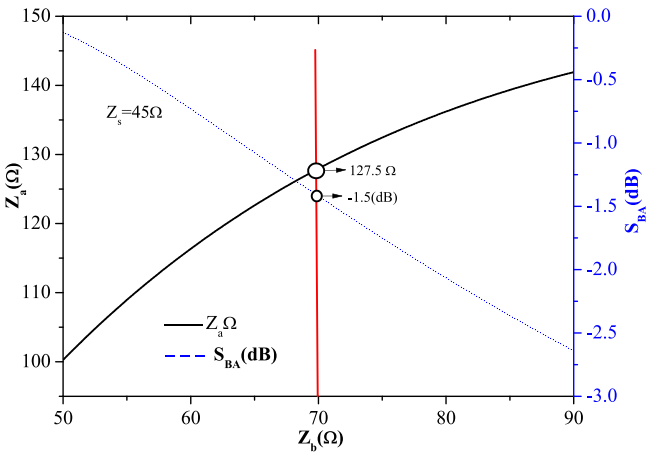

FIGURE 6. Variation of Z_a with S_{BA} (dB) with change in Z_b for fixed value of Z_s to obtain the impedance solution for unequal split.

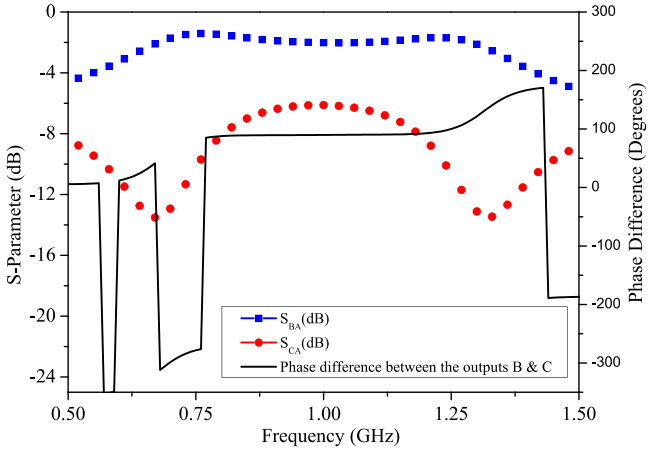

FIGURE 7. S-parameters and phase difference at the power splits ports of the proposed unequal split four branch line hybrid coupler.

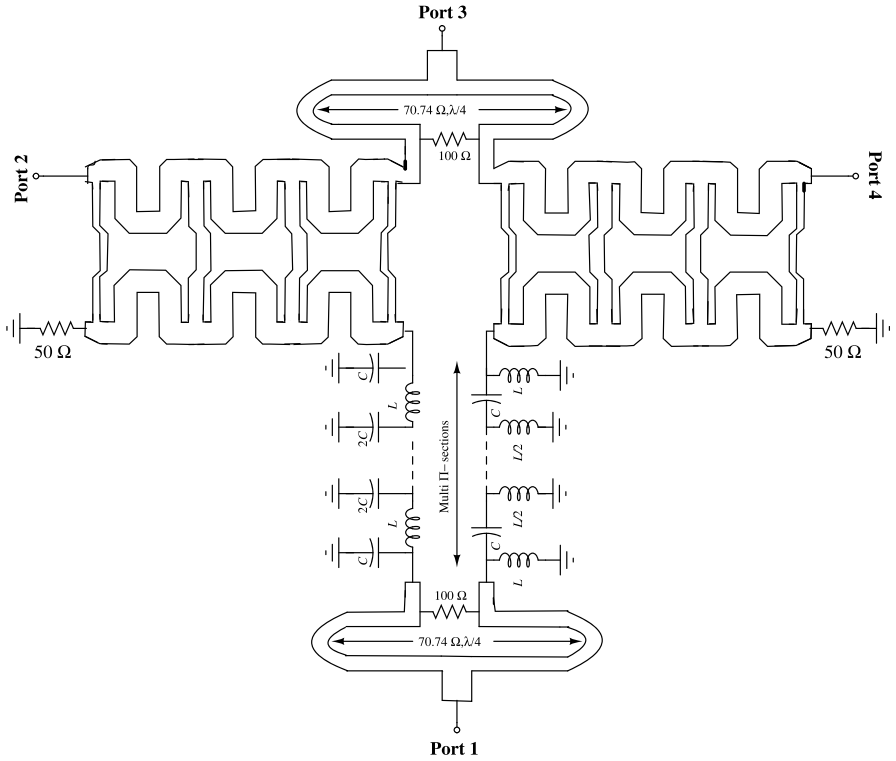

FIGURE 8. Complete schematic diagram of the proposed class of asymmetric hybrid coupler employing N-section phase shift filters and unequal split four branch line hybrid couplers.

1 GHz, a tight coupling close to 2 dB of the four section branch line hybrid coupler is obtained over the frequency range from 0.75 GHz to 1.25 GHz. Since four branch line hybrid couplers increase the overall size of the circuit, meandered lines have been used to realize all sections and lines of the entire hybrid coupler, and its layout is shown in Fig. 5. The simulated results discussed above are for this layout with reduced size.

TABLE 4. Impedance, widths, and lengths of lines used in the unequal split four branch line hybrid coupler for FR4.

	Line a	Line b	Line s
Z	127.56 Ω	70.01 Ω	44.98 Ω
W	0.29 mm	1.6 mm	3.58 mm
L	44.223 mm	42.22 mm	40.77 mm

3. SIMULATED AND MEASURED RESULTS

The diagram of the complete proposed asymmetric hybrid coupler, incorporating the class of N-section phase shifter, four branch line hybrid coupler, and Wilkinson divider and combiner, is shown in Figure 8. The entire hybrid is designed and laid out on an FR4 substrate ($\epsilon_r = 4.4$, $h = 1.6$ mm, $\tan\delta = 0.02$). Figure 9 shows the photographs of fabricated

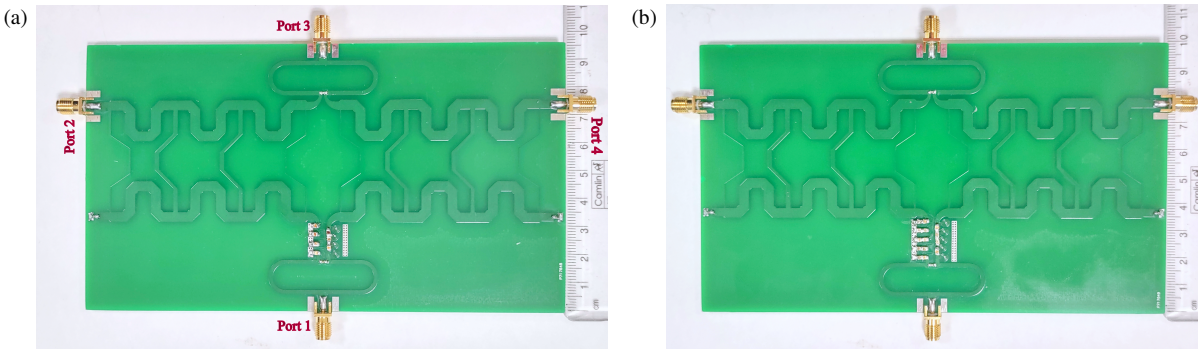

FIGURE 9. Photographs of the (a) $N = 3$, (b) $N = 4$ asymmetric hybrid couplers fabricated on FR4 substrate.

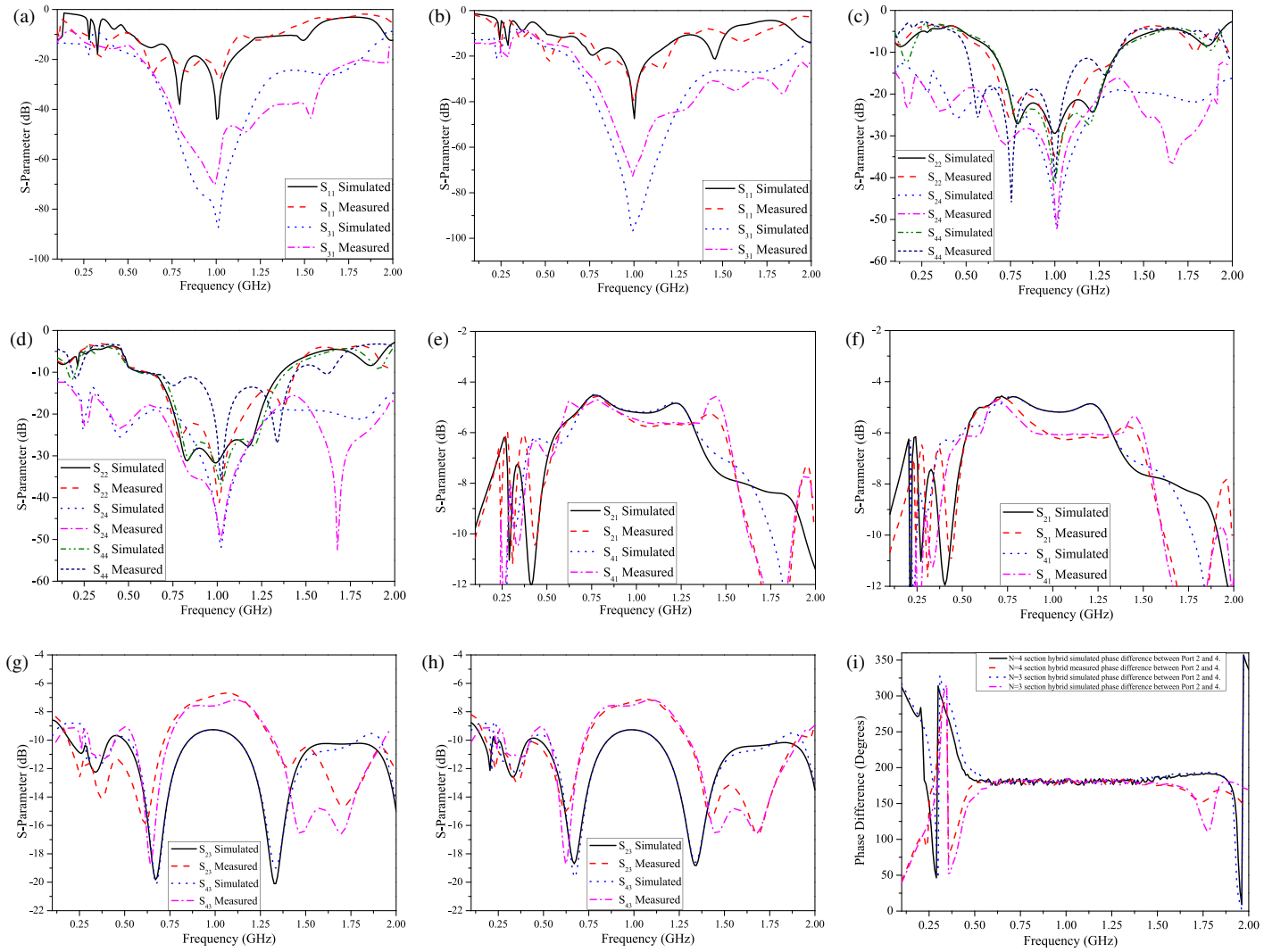

FIGURE 10. S_{11} and S_{31} of (a) $N = 3$, (b) $N = 4$ section hybrid, S_{22}, S_{24} and S_{44} of (c) $N = 3$, (d) $N = 4$ section hybrid, S_{21} and S_{41} of (e) $N = 3$, (f) $N = 4$ section hybrid, S_{23} and S_{43} of (g) $N = 3$, (h) $N = 4$ section hybrid, (i) phase difference between Port 2 and Port 4 of $N = 3$ and $N = 4$ section hybrid.

hybrid coupler microstrip printed circuit boards (PCBs), on an FR4 substrate. Figure 10 presents the simulated and measured S-parameters of the proposed class of hybrids with N sections of the phase shift filter circuit employed. It includes two prototypes of the hybrids for $N = 3$ and $N = 4$. All the simulations are carried out in Cadence AWR Microwave Office using the mixed mode simulations involving AXIEM tools. The S-parameters of the circuit were measured using Keysight E5071C VNA, with 2-port calibration and de-embedding till the SMA connector ports. All simulations and measurements are carried out between 0.1 and 2 GHz, with bandwidth calculations based on a center frequency of 1 GHz.

TABLE 5. Comparison of the proposed class of asymmetric N-section hybrid couplers with previously reported papers.

Ref.	Technique Used	f_o (GHz)	FBW (%)	C (dB)	I (dB)	Peak Isolation (dB)	Size
[2]	Generalized coupling slot	2	53	20	≥ 60	72	$0.23\lambda_g \times 0.04\lambda_g$
[3]	Phase control unit	3.5	17.1	3	≥ 10	20	$0.65\lambda_g \times 0.76\lambda_g$, $0.49\lambda_g \times 0.92\lambda_g$, $0.42\lambda_g \times 0.63\lambda_g$
[4]	Lumped bridged-T amplitude equalizer	11	163.36	20	≥ 40	42	$0.23\lambda_g \times 0.135\lambda_g$
[5]	Printed RGW technology	30	26.5	3	≥ 15	35	$1.2\lambda_g \times 1.2\lambda_g$
[7]	Tunable phase shifting unit	1	20	3	≥ 12	22	$0.18\lambda_g \times 0.24\lambda_g$
[9]	BTSE 180° hybrid	3	12	3	≥ 30	37.8	$0.95\lambda_g \times 0.95\lambda_g$
[11]	Phase reconfigurable transmission line	2.4	16	6.2	≥ 10	25	Not mentioned
[13]	Three folded coupled lines	2	55	3	≥ 15	70	$0.39\lambda_g \times 0.68\lambda_g$
[15]	RGW technology	18.5	40	3	≥ 20	40	$2\lambda_g$ long
[16]	Inclined longitudinal slots in between two layers of coupler	28	7.1	4	≥ 14	52	$\lambda_g \times 0.6\lambda_g$
[18]	Circular patch	4.21/6.39	20.9/9.5	3	≥ 20	45	$0.53\lambda_g \times 0.53\lambda_g$
[22]	Rectangular pieces with 9 squares in the center	2.27	22.22	3	≥ 15	23	$18.36\lambda_g$ long
[23]	Two LPFs realized using stubs	1.8	11.11	3	≥ 20	40	$0.011\lambda_g^2$
[24]	Lumped elements with limited quality factor	0.5	20	3	≥ 20	22	$0.038\lambda_g \times 0.038\lambda_g$
This work	$N = 3$ section phase shift filter circuit	1	73.68	≤ 6	≥ 15	66.5	$0.56\lambda_g \times 1.03\lambda_g$
This work	$N = 4$ section phase shift filter circuit	1	91.89	≤ 6	≥ 15	72.7	$0.59\lambda_g \times 1.03\lambda_g$

$*$ f_o = Center frequency, FBW = Fractional bandwidth, C = Coupling, I = Isolation.

For the class of N-section hybrids, the reference measures are taken as follows:

1. Port return losses S_{11} better than 10 dB, S_{22} and S_{44} better than 10 dB.
2. Isolation (corresponding to S_{31}) better than 15 dB.
3. Coupling and insertion loss (corresponding to S_{21} and S_{41} respectively), better than 6 dB.
4. Isolation (corresponding to S_{24}) better than 10 dB.
5. Phase difference between output Ports 2 and 4 approximately 180°.

Furthermore, S_{23} and S_{43} are presented in Figures 10(g) and (h) highlighting the useful application of the hybrid (presented in Section 3.2). With these parameters, the $N = 3$ hybrid exhibits a frequency range from 0.6 GHz to 1.3 GHz, equating to a percentage bandwidth of 73.68% for the above parameters (1, 2 and 3). In addition to these parameters, the $N = 3$ hybrid shows a peak isolation of 87.4 dB in simulation and 66.5 dB in measurement at the center frequency of 1 GHz. The $N = 4$ hybrid achieves a frequency range from 0.5 GHz to 1.35 GHz, resulting in a percentage bandwidth of 91.89% for the above parameters (1, 2, and 3). Furthermore, the $N = 4$ hybrid shows a peak isolation of 96.8 dB in simulation and 72.7 dB in measurement at the center frequency of 1 GHz. There is a close agreement between the simulated and measured responses, with some minor deviations observed. These differences are primarily attributed to fabrication tolerances, substrate non-uniformity, influence of soldering imperfections, connector transitions, use of partial lumped and partial planar components in designing phase shifter circuit for compact design which are difficult to fully model during simulation. Despite these minor discrepancies, overall there is good agreement between the simulated and measured results. It is observed and verified that multiple sections of the phase shift filter circuit achieve increased bandwidth with each additional section, i.e., increased N.

3.1. Comparison with Previously Reported State of the Art

Table 5 shows the comparison of the proposed four hybrids and their parameters with previously reported couplers and hybrids. The coupler proposed in [4] exhibits broad operating bandwidth and high isolation; however, it results in loose coupling. The

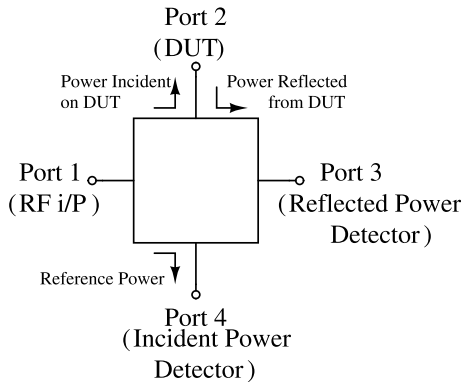

FIGURE 11. Block diagram of proposed asymmetric microstrip hybrid coupler working as an VNA testset.

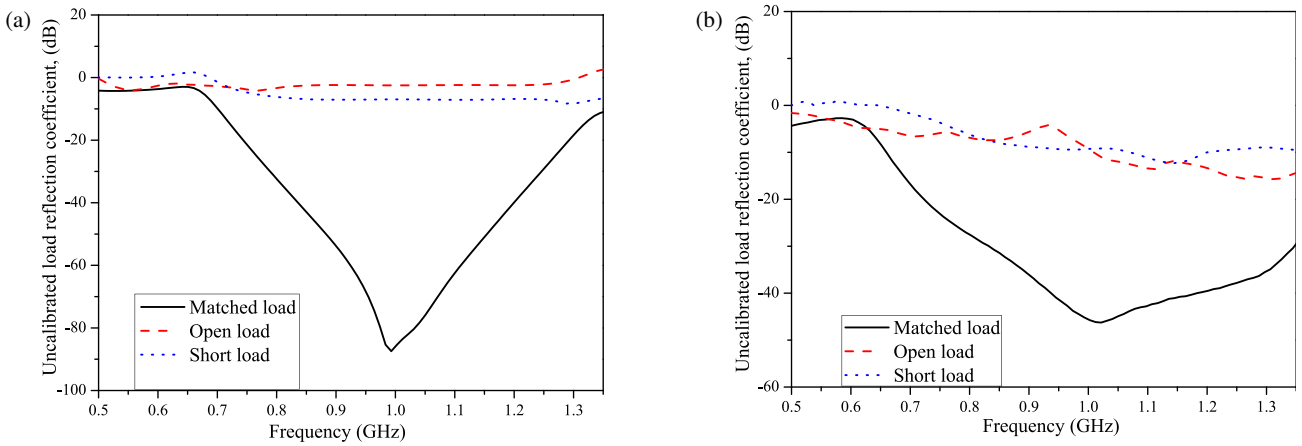

FIGURE 12. Uncalibrated reflection coefficients for matched, open and short loads computed from (a) simulated, (b) measured S-parameter of hybrid coupler shown in Figure 8.

hybrid couplers reported in [9, 15, 18] exhibit both 3 dB coupling and high isolation better than 20 dB; however, the hybrid proposed in this paper offers a broader bandwidth than them, while maintaining tight coupling. The layout of the proposed design minimizes potential interference, leading to improved system reliability. Furthermore, at higher frequencies, the layout size of the hybrid coupler is reduced which ensures scalability.

3.2. Application of the Proposed Hybrid Coupler

Figure 11 shows an application of the proposed coupler as a vector network analyzer (VNA) test set. High isolation and dynamic range are the essential requirements for a network analyzer test set [33]. Load dynamic range is the difference between reflection coefficient of perfectly matched 50 Ω load and mismatched open/short loads, assuming continuous incident power on the load. The working of the proposed hybrid coupler is as follows: when an RF signal is applied to Port 1, the Wilkinson power divider and phase shifter generate two outputs of equal amplitude but with a 180° phase difference. These signals are fed to Ports 2 and 4 via an unequal-split branch-line hybrid, which adds a 90° phase shift while maintaining the 180° phase difference between them. The hybrid also provides isolation between Ports 2 and 4 and contributes to wide bandwidth due to its multi-branch structure. Port 4 can be terminated with a matched 50 Ω load, serving as a reference port. If the device under test (DUT) connected at Port 2 is perfectly matched, the reflected signals from Ports 2 and 4 undergo perfect phase cancellation through the Wilkinson combiner, resulting in minimal signal at Port 3. However, any mismatch at Port 2 leads to imperfect cancellation, and large reflected power appears at Port 3, which can be monitored by a detector. S-parameter magnitudes of the stand-alone test set can be used to calculate the uncalibrated reflection coefficient Γ_L (dB) of the DUT. It can be derived using following equations [34]:

$$\text{Power reflected from load (dB)} = S_{31}\,\text{(dB)} - S_{32}\,\text{(dB)} \quad (27)$$

$$\text{Power incident on load (dB)} = S_{41}\,\text{(dB)} \quad (28)$$

$$\Gamma_L\,\text{(dB)} = [S_{31}\,\text{(dB)} - S_{32}\,\text{(dB)}] - S_{41}\,\text{(dB)} \quad (29)$$

This behavior makes the proposed coupler suitable for the use in vector network analyzer (VNA) test sets. This application is tested for designed prototype $N = 4$. Figure 12(a) shows simulated uncalibrated reflection coefficient, and Figure 12(b) shows measured uncalibrated reflection coefficient for matched, open and short loads. The simulated results achieve a peak dynamic range of 82.7 dB around center frequency 1 GHz and over 15 dB for 0.75–1.3 GHz band, while the measured performance remains robust above 15 dB for frequency range from 0.7 GHz to 1.35 GHz with peak dynamic range 36.4 dB around 1 GHz.

4. CONCLUSION

In this paper, a class of asymmetric, tightly coupled enhanced bandwidth, high isolation microstrip hybrid couplers is presented. High isolation and broad bandwidth are achieved by incorporating a generalized N-section phase shift filter circuit. The complete design process for an N-section phase shifter is developed and presented in the paper. Further, to obtain tight coupling above 6 dB, over a broad band, a multi-branch line hybrid coupler with unequal split is designed and used. It is established that a noticeable improvement in bandwidth is obtained with each additional phase shift filter section. To validate the hypothesis, two prototypes with $N = 3$ and $N = 4$ are designed, simulated, fabricated, and measured for a center frequency of 1 GHz. Fractional bandwidths of 73.68% and 91.89% are achieved for the two cases, respectively. Maximum frequency range from 0.5 GHz to 1.35 GHz is achieved for $N = 4$ with peak isolation 72.7 dB at center frequency 1 GHz. The outlined design methodology for the proposed class of hybrids is scalable and adaptable to any desired frequency band by employing suitable substrate respectively. In this case, the fabrication on an FR4 substrate makes the proposed designs suitable for use in low cost applications. The scalable and frequency-flexible design approach makes the proposed class of hybrid couplers highly suitable for modern microwave systems such as VNA test set, applications in radar, communication networks, and phased array antennas [35, 36].

ACKNOWLEDGEMENT

This work is supported by Anusandhan National Research Foundation Government of India under grant CRG/2023/000306.

REFERENCES

[1] Santiko, A. B., Y. P. Saputera, and Y. Wahyu, "Design and implementation of three branch line coupler at 3.0 GHz frequency for S-band radar system," in *2016 22nd Asia-Pacific Conference on Communications (APCC)*, 315–318, Yogyakarta, Indonesia, 2016.

[2] Hu, G., G. Wang, N. Yang, and Q. Zhang, "Multiobjective optimization design of microstrip directional coupler with generalized coupling slots," *IEEE Transactions on Microwave Theory and Techniques*, Vol. 72, No. 1, 252–261, 2024.

[3] Pan, Y. F., Y. Yang, W. S. Chan, S. Y. Zheng, and W. Shang, "A simple and universal phase control method for designing directional couplers with adjustable phase difference slope and high linearity," *IEEE Transactions on Microwave Theory and Techniques*, Vol. 71, No. 9, 3882–3895, 2023.

[4] Li, S., L. Ma, L. Wang, B. Wu, Y. Cheng, X. Lei, F. Liu, and G. J. Cheng, "An ultrawideband GaAs MMIC microstrip directional coupler with high directivity and very flat coupling," *IEEE Transactions on Microwave Theory and Techniques*, Vol. 70, No. 4, 2271–2279, 2022.

[5] Ali, M. M. M., M. S. El-Gendy, M. Al-Hasan, I. B. Mabrouk, A. Sebak, and T. A. Denidni, "A systematic design of a compact wideband hybrid directional coupler based on printed RGW technology," *IEEE Access*, Vol. 9, 56 765–56 772, 2021.

[6] Wang, Z.-B., X. Wei, H.-P. Fang, H.-M. Zhang, and Y.-R. Zhang, "A compact and broadband directional coupler for high-power radio frequency applications," *IEEE Microwave and Wireless Components Letters*, Vol. 30, No. 2, 164–166, 2020.

[7] Zhu, H. and A. M. Abbosh, "A compact tunable directional coupler with continuously tuned differential phase," *IEEE Microwave and Wireless Components Letters*, Vol. 28, No. 1, 19–21, 2018.

[8] Zheng, Y., Y. Wu, W. Wang, and L. Pan, "Uniplanar compact 180° hybrid coupler with fast and accurate wide power-division ratio switching ranges and enhanced bandwidth," *IEEE Transactions on Microwave Theory and Techniques*, Vol. 71, No. 12, 5470–5481, 2023.

[9] Huang, F., L. Zhu, and H. Zhang, "Balanced-to-single-ended filtering 180° hybrids with arbitrary power-division ratio," *IEEE Transactions on Microwave Theory and Techniques*, Vol. 71, No. 5, 2082–2090, 2023.

[10] Zhu, H., T. Zhang, and Y. J. Guo, "Wideband hybrid couplers with unequal power division/arbitrary output phases and applications to miniaturized Nolen matrices," *IEEE Transactions on Microwave Theory and Techniques*, Vol. 70, No. 6, 3040–3053, 2022.

[11] Chu, H. N., H.-C. Liao, G.-Y. Li, and T.-G. Ma, "Novel phase reconfigurable synthesized transmission line and its application to reconfigurable hybrid coupler," in *2017 12th European Microwave Integrated Circuits Conference (EuMIC)*, 337–340, Nuremberg, Germany, 2017.

[12] Deng, T., K. Y. Chan, Y. Fu, and R. Ramer, "An analytical design method for a wideband differential waveguide directional coupler with de-embedding analysis," *IEEE Transactions on Instrumentation and Measurement*, Vol. 73, 1–9, 2024.

[13] Pan, L., Y. Wu, W. Wang, Y. Zheng, and Y. Liu, "A symmetrical broadband tight-coupled directional coupler with high directivity using three-folded-coupled lines," *IEEE Transactions on Circuits and Systems II: Express Briefs*, Vol. 69, No. 9, 3744–3748, 2022.

[14] Buesa-Zubiria, A. and J. Esteban, "Design of broadband doubly asymmetrical branch-line directional couplers," *IEEE Transactions on Microwave Theory and Techniques*, Vol. 68, No. 4, 1439–1451, 2020.

[15] Nasr, M. A. and A. A. Kishk, "Analysis and design of broadband ridge-gap-waveguide tight and loose hybrid couplers," *IEEE Transactions on Microwave Theory and Techniques*, Vol. 68, No. 8, 3368–3378, 2020.

[16] Harini, K., T. R. G. Babu, R. Praveena, G. Sudha, K. G. Kannan, and J. Gnanasoundharam, "Design of compact folded SIW hybrid coupler for Ka band application," in *2022 Third International Conference on Intelligent Computing Instrumentation and Control Technologies (ICICICT)*, 1693–1697, Kannur, India, 2022.

[17] Liu, H., S. Fang, Z. Wang, and S. Fu, "Analysis and implementation of a dual-band coupled-line trans-directional coupler," *IEEE Transactions on Circuits and Systems II: Express Briefs*, Vol. 67, No. 3, 485–490, 2020.

[18] Zhang, G., F. Jiao, S. Liu, L. Zhu, S. Wang, Q. Zhang, and J. Yang, "Compact single- and dual-band filtering 180° hybrid couplers on circular patch resonator," *IEEE Transactions on Microwave Theory and Techniques*, Vol. 68, No. 9, 3675–3685, 2020.

[19] Wu, X. and L.-P. Shen, "A miniaturized microstrip branch-line hybrid coupler using two sections and coupled-lines," in *2021 IEEE International Symposium on Antennas and Propagation and USNC-URSI Radio Science Meeting (APS/URSI)*, 1741–1742, Singapore, 2021.

[20] Wu, X. and L.-P. Shen, "Compact ultra-wideband microstrip 3 dB branch-line coupler using coupled-lines," in *2022 IEEE International Symposium on Antennas and Propagation and USNC-URSI Radio Science Meeting (AP-S/URSI)*, 1462–1463, Denver, CO, USA, 2022.

[21] Madhuri, A. N., A. Bharathi, and M. Swetha, "X band miniaturized 90° hybrid coupler," in *2022 IEEE Wireless Antenna and Microwave Symposium (WAMS)*, 1–5, Rourkela, India, 2022.

[22] İmeci, M. Y., B. Tütüncü, and S. T. İmeci, "A 3-dB 90 degrees microstrip hybrid directional coupler at 2.27 GHz," *AEU — International Journal of Electronics and Communications*, Vol. 163, 154606, 2023.

[23] Nouri, L., S. I. Yahya, and A. Rezaei, "Design and fabrication of a compact branch-line hybrid coupler with a balanced phase using a new microstrip structure for GSM applications," *AEU — International Journal of Electronics and Communications*, Vol. 161, 154529, 2023.

[24] Beigizadeh, M., R. Dehghani, and A. Nabavi, "Analysis and design of a lumped-element hybrid coupler using limited quality factor of components," *AEU — International Journal of Electronics and Communications*, Vol. 82, 312–320, 2017.

[25] Young, L., "Synchronous branch guide directional couplers for low and high power applications," *IRE Transactions on Microwave Theory and Techniques*, Vol. 10, No. 6, 459–475, 1962.

[26] Levy, R. and L. F. Lind, "Synthesis of symmetrical branch-guide directional couplers," *IEEE Transactions on Microwave Theory and Techniques*, Vol. 16, No. 2, 80–89, 1968.

[27] Saleh, A. A. M., "Planar electrically symmetric N-way hybrid power dividers/combiners," *IEEE Transactions on Microwave Theory and Techniques*, Vol. 28, No. 6, 555–563, 1980.

[28] Parisi, S. J., "180 degrees lumped element hybrid," in *IEEE MTT-S International Microwave Symposium Digest*, 1243–1246, Long Beach, CA, USA, 1989.

[29] Hamming, R., *Numerical Methods for Scientists and Engineers*, Courier Corporation, 2012.

[30] Kawabe, K., H. Koyama, and K. Shirae, "Planar inductor," *IEEE Transactions on Magnetics*, Vol. 20, No. 5, 1804–1806, 1984.

[31] Ghosh, D. and G. Kumar, "A four branch microstrip coupler with improved bandwidth and isolation," in *2015 Twenty First National Conference on Communications (NCC)*, 1–6, Mumbai, India, 2015.

[32] Frickey, D. A., "Conversions between S, Z, Y, H, ABCD, and T parameters which are valid for complex source and load impedances," *IEEE Transactions on Microwave Theory and Techniques*, Vol. 42, No. 2, 205–211, 1994.

[33] Ghosh, D. and G. Kumar, "Broadband, partially unilateral active testset for network analyser," *Electronics Letters*, Vol. 52, No. 14, 1266–1268, 2016.

[34] Tirmanwar, S. and D. Ghosh, "Single chip broadband testset for network analyzers," in *2020 URSI Regional Conference on Radio Science (URSI-RCRS)*, 1–4, Varanasi, India, 2020.

[35] Afroz, S. and K.-J. Koh, "90° hybrid-coupler based phase-interpolation phase-shifter for phased-array applications at W-band and beyond," in *2016 IEEE MTT-S International Microwave Symposium (IMS)*, 1–4, San Francisco, CA, USA, 2016.

[36] Ahmed, F. H., R. Saad, and S. K. Khamas, "Flexible phase-reconfigurable branch line coupler for millimeter-wave phased array antenna," in *2024 18th European Conference on Antennas and Propagation (EuCAP)*, 1–5, Glasgow, United Kingdom, 2024.